4th International Conference on Water Resources and Arid Environments (ICWRAE 4): 167-183
5-8 December 2010, Riyadh, Saudi Arabia

Hydro-Geological and Geophysical Investigation in an Area Located at Northeastern Part of Greater Cairo, Egypt

Sultan Awad Sultan Araffa

National Research Institute of Astronomy and Geophysics, 11722, Helwan, Cairo, Egypt

Abstract: The present study aims to investigate the shallow and deeper section to delineate the groundwater aquifer and structural elements which dissect the study area located at the north eastern part of Greater Cairo, Egypt. Added, the study aims to define the depth to a basaltic sheet and evaluating the quality of groundwater through interpretation of the geophysical, geological and boreholes data. Geophysical tools such as vertical electrical soundings (VES), dipole-dipole and magnetic data have been applied to accomplish this goal. Forty one vertical electrical soundings (VES) have been measured and interpreted using 3-D VES inversion program. The results of inversion indicated that the area consists of Quaternary deposits at shallow depths (5-20m), Miocene deposits found at depths range from 5.5m to more than 80m and the groundwater aquifer at depth ranging from 50 to 200 m. Five dipole-dipole sections have been measured to investigate the shallow part of the subsurface section. The data were inverted using RES2DINV program and the inverted data were represented through 3-D slices at depths ranging from 1.1 to 11.1m. Results of the inverted data reflect that the shallow part of the subsurface section is represented very low resistivity at the western part of the area; which corresponds to the Nile silt and Nile mud of Quaternary deposits. However, the eastern part showed high resistivities that correspond to sand and sandstone of Quaternary and Miocene deposits. Two hundred-twenty two ground magnetic stations were measured and interpreted to identify the depth to the upper surface of the basaltic sheet and to determine the fault elements which dissect the area. The results indicated that the eastern part is engaged by deep depths to the basalts; ranging from 175 to 250 m and the western part reveals relatively shallower depths ranging from 75 to 150 m. In addition, the area is dissected by fault elements of NW-SE, NE-SW and N-S trends. The hydrogeological data indicated that the hydraulic conductivity is ranging between 0.061 to 1.427 cm/min, water table level ranging between 13.2-14.1 m and porosity percentage ranging from 13 to 23 %. The hydrochemistry of the groundwater analysis indicated that the salinity of water is ranging between 550-2200 mg/l and the water type is Na-Cl-SO4 for most boreholes.

Key words: Hydro-Geological • Geophysical Investigation • Egypt

INTRODUCTION

Resistivity is a geophysical method that images the earth by measuring the potential generated by injecting DC electricity into ground. The resulting geoelectrical image show the distribution of the earth' resistivity, which can be related to different soil and rock type. Many authors discussed the theory and application of resistivity method such as [1-3]. Electrical resistivity imaging (ERI) has become an important engineering and environmental site investigation tool, [4]. Resistivity images are created by inverting hundreds to thousands of individual resistivity measurements (e.g., [5,6] to produce an approximate model of the subsurface resistivity. [7] illustrated a simple inversion algorithm that uses a data bank of forward solutions for a certain class of 3D models. [8] proposed an inversion method based on the Born approximation [9,10] used 1-D and 3D resistivity inversion for groundwater exploration and engineering geology. In the present study 2D dipole-dipole, 3D inversion for 1-D VES and ground magnetic survey were carried at the area located at the north of Abu Zabal city and at distance of 2km west Ismailia Canal (branch of River Nile) and cover an area of 0.5 km^2 to investigate stratigraghy, structures and groundwater occurrences (Fig.1).

Geology of the area: The surface geology was described by [11] as shown in Figure 1 where most the study area covered by Quaternary deposits which consist

Corresponding Author: Sultan Awad Sultan Araffa, National Research Institute of Astronomy and Geophysics, 11722, Helwan, Cairo, Egypt

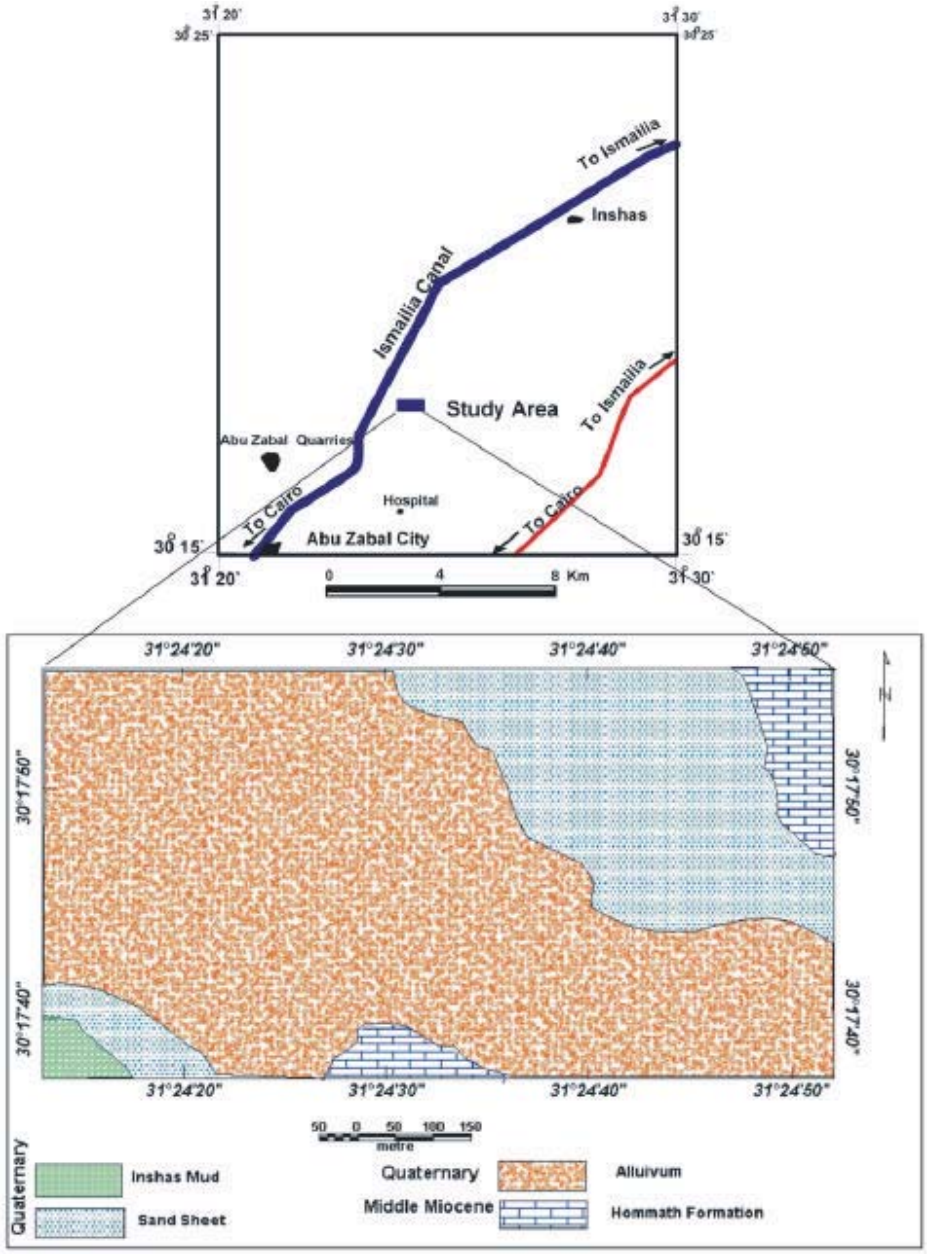

Fig. 1: Location and geological map of the area

of alluvium, sand sheet and Nile silt and Nile mud. The Miocene deposits occupied the northeastern and southern parts of the area which represented by Hommath formation and composed of sandy limestone, sand, sandstone and clay (Fig. 1). Stratigraphically, the drilled boreholes reflect the rock types with depth in the area. The Quaternary deposits are represented Nile silt and mud, loose sands, sandstone, gravel with a thickness ranging from few meters to 20 m. The Miocene deposits are expressed limestone, sand, sandstone, clay and calcareous sandstone. The Oligocene deposits are represented by basaltic flow and sand and sandstone of Gabal Ahmar Formation. The depth of the upper surface of the basaltic flow ranging from 75 m at borehole no.7 to 128 m at borehole no.9. Gabal Ahmar Formation appeared at the borehole no.13 at depth of 113.5 m to the end of the borehole at depth of 202 m (Fig. 2).

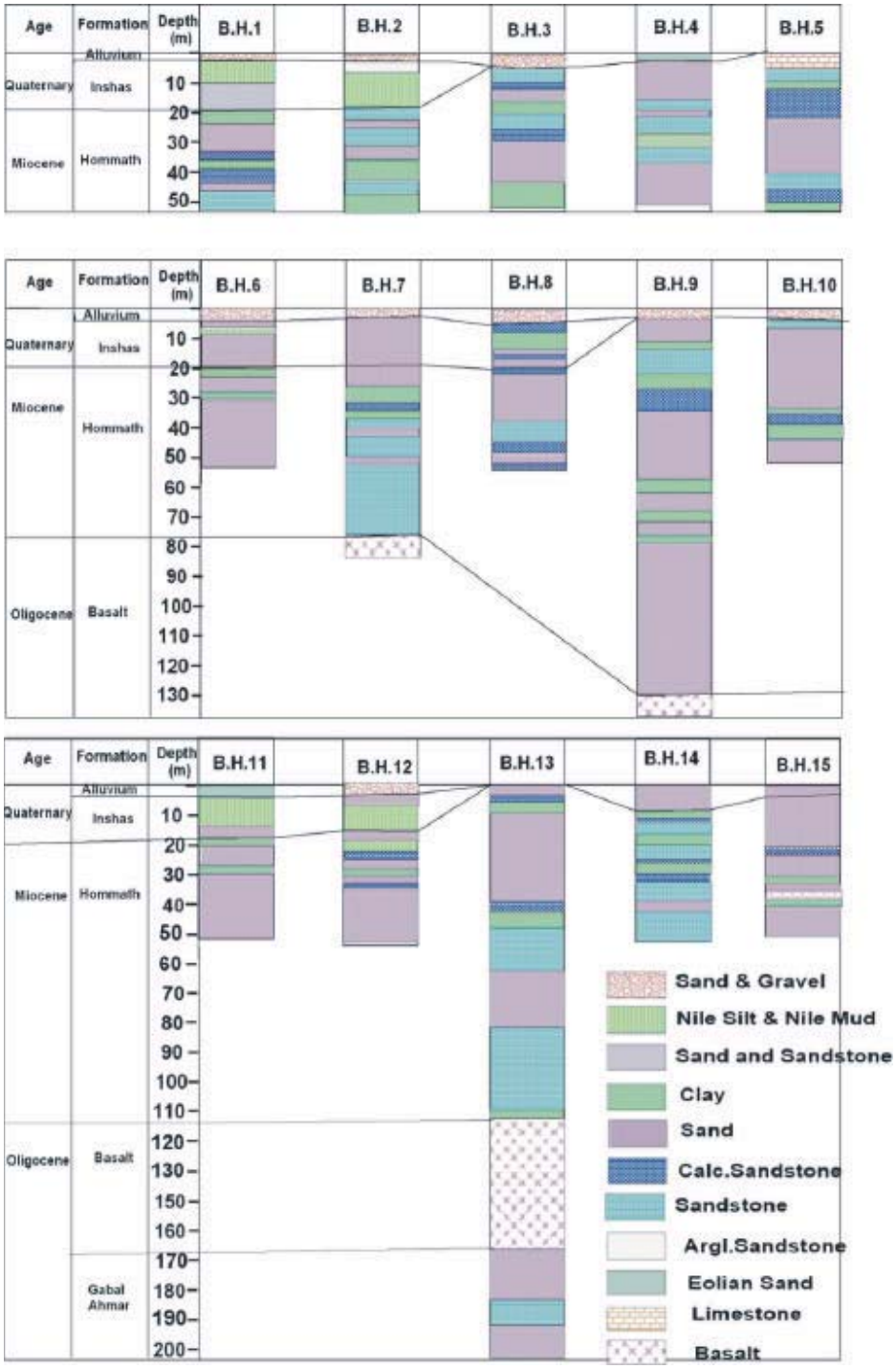

Fig. 2: Boreholes description

MATERIALS AND METHODS

Shallow Geoelectrical Investigation Tools: The shallow investigation tools in the present study were represented by measuring five dipole dipole sections. The length of each section is one kilometer and spacing between sections is 125 m (Fig.3). The spacing between current electrodes and potential electrodes is a multiple of the

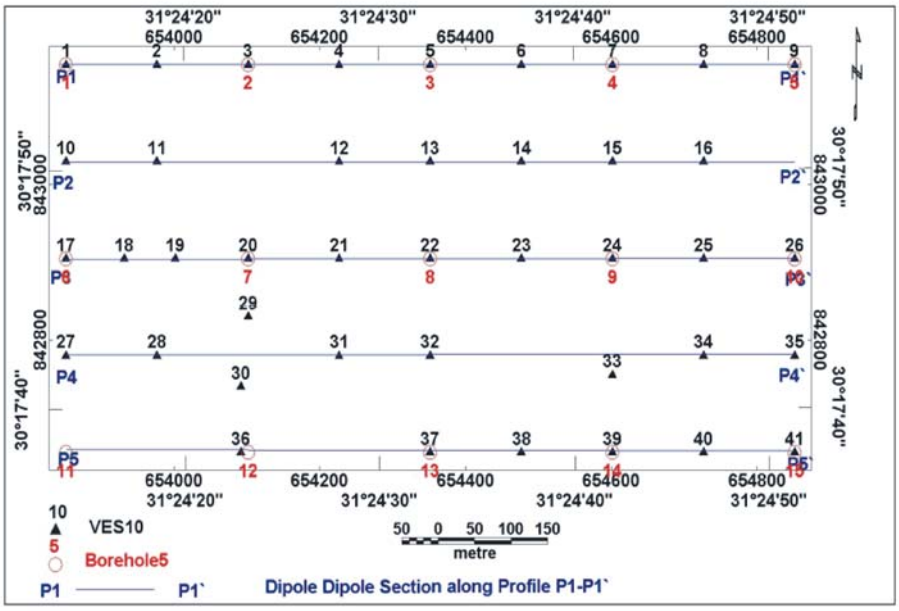

Fig. 3: Location map of geophysical measurements and boreholes

electrode spacing (*a*), in the present study (*a*) is equal 5 m. The depth of penetration is a function of the distance *a* [12,6]. The dipole-dipole profiles were inverted using the RESINV2D software which produced an image of the electrical resistivity distribution in the subsurface based on a regularization algorithm [6]. The inverted dipole-dipole section along profile P1-P1` (Fig.4a) exhibits large variation in resistivities where the first half of the section divided into two parts, the first part is shallow depth ranging from 1.1 to 4 m and shows moderate resistivities ranging from 10 to 50 ohm.m corresponding to alluvium deposits, the second part is at depth ranging from 4 to 11.1 m and exhibits very low resistivities ranging from 1 to 10 ohm.m corresponding to Nile silt and Nile mud. The second half of the section reflects very high resistivities up to 750 omh.m corresponding to sand sheet and sandstone, the end part of the section reveals moderate and low resistivities corresponding to limestone and clay respectively. The second dipole-dipole section along profile P2-P2` (Fig.4b) reveals low resistivities at the first half of the section according to alluvium and Nile silt and Nile mud, the second half reveals high resistivities corresponding to sand and sandstone with some clay of low resistivities. The dipole-dipole section along profile P3-P3` (Fig.4c) indicates low resistivities for most section corresponding to alluvium and Nile silt and Nile mud, the last part of the section reveals high resistivities at depth ranging from 4 to 11.1 m corresponding to sand and sandstone. The dipole-dipole section along profile P4-P4` (Fig.4d) shows variation in resistivities ranging from low values according to clay, Nile silt and Nile mud to very high rsistivities of sandstone and sand. The last section along profile P5-P5` (Fig.4e) exhibits at the first and mid part from distance 500 to 720 m a very low resistivities ranging from 1-10 ohm.m according to clay, Nile silt and Nile mud, the mid part at distance from 250 to 500 m and the last part of the section reveals very high resistivities corresponding to sand and sandstone.

D Representation for Dipole-Dipole Data: The Dipole-dipole data were represented by 3D slices at different depths of 1.1, 3.3, 5.7, 8.2 and 11.1 m (Fig.5). The slices at depth 1.1 and 3.3 m reveal low resistivities ranging from 5 to 100 ohm.m at the most of the area corresponding to alluvium deposits, the northeastern and southeastern parts are occupying by very high resistivity up to 750 ohm.m. The slice at depth of 5.7 m shows very low and low resistivities at the western half of the area corresponding to clay, Nile silt and Nile mud, the eastern half of the area is occupying by high and very high resistivities for sand and sandstone. The slices at depth 8.2 and 11.1m exhibit very low resistivities corresponding to Nile silt and Nile mud at the western part of the area, the eastern part is occupying by sand and sandstone of high resistivities.

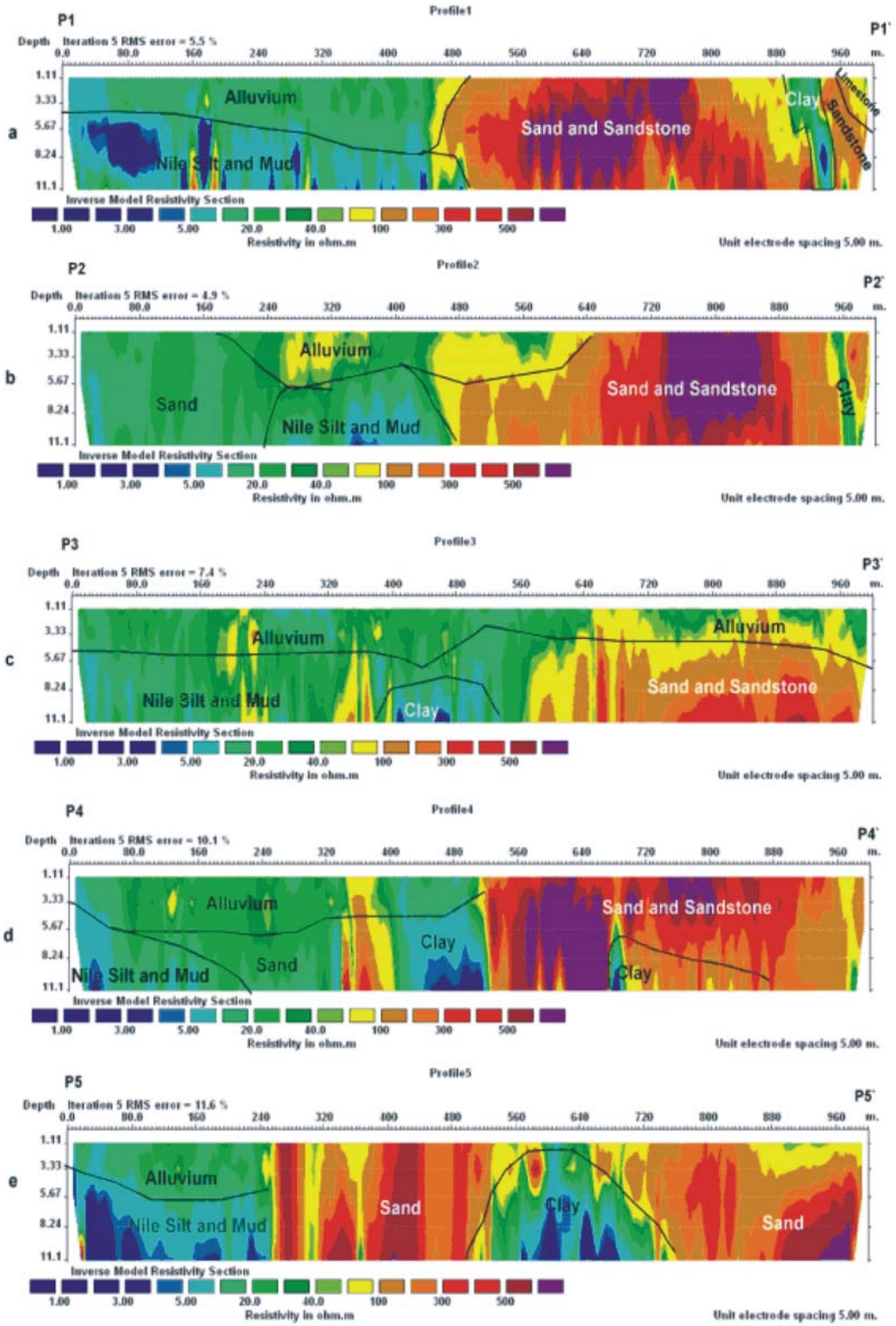

Fig. 4: Dipole-dipole section inverted using RES2DINV program; a: for profile P1-P1`, b: for profile P2-P2`, c: for profile P3-P3`, D: for profile P4-P4` and e: for profile P5-P5`.

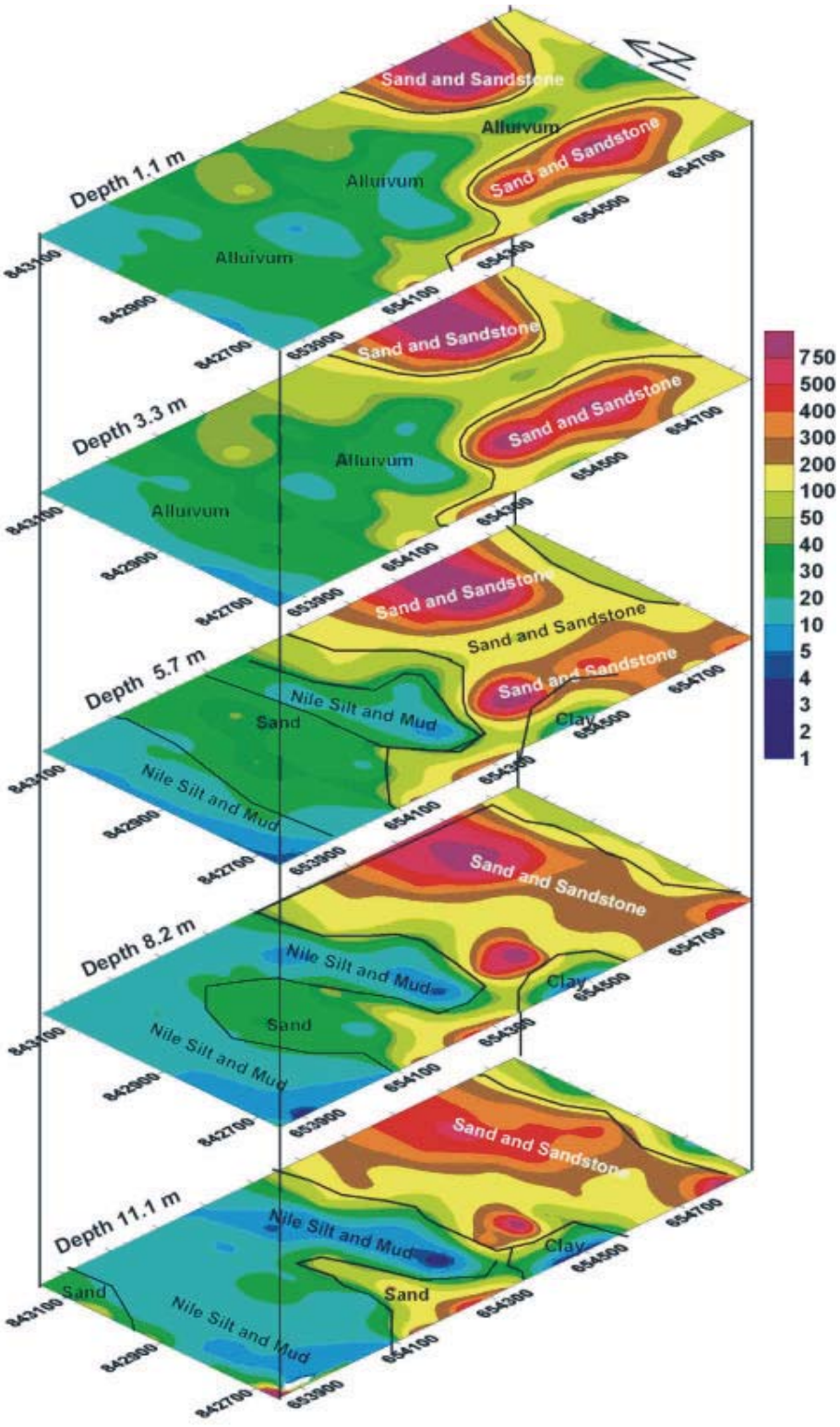

Fig. 5: 3D representation for dipole-dipole data

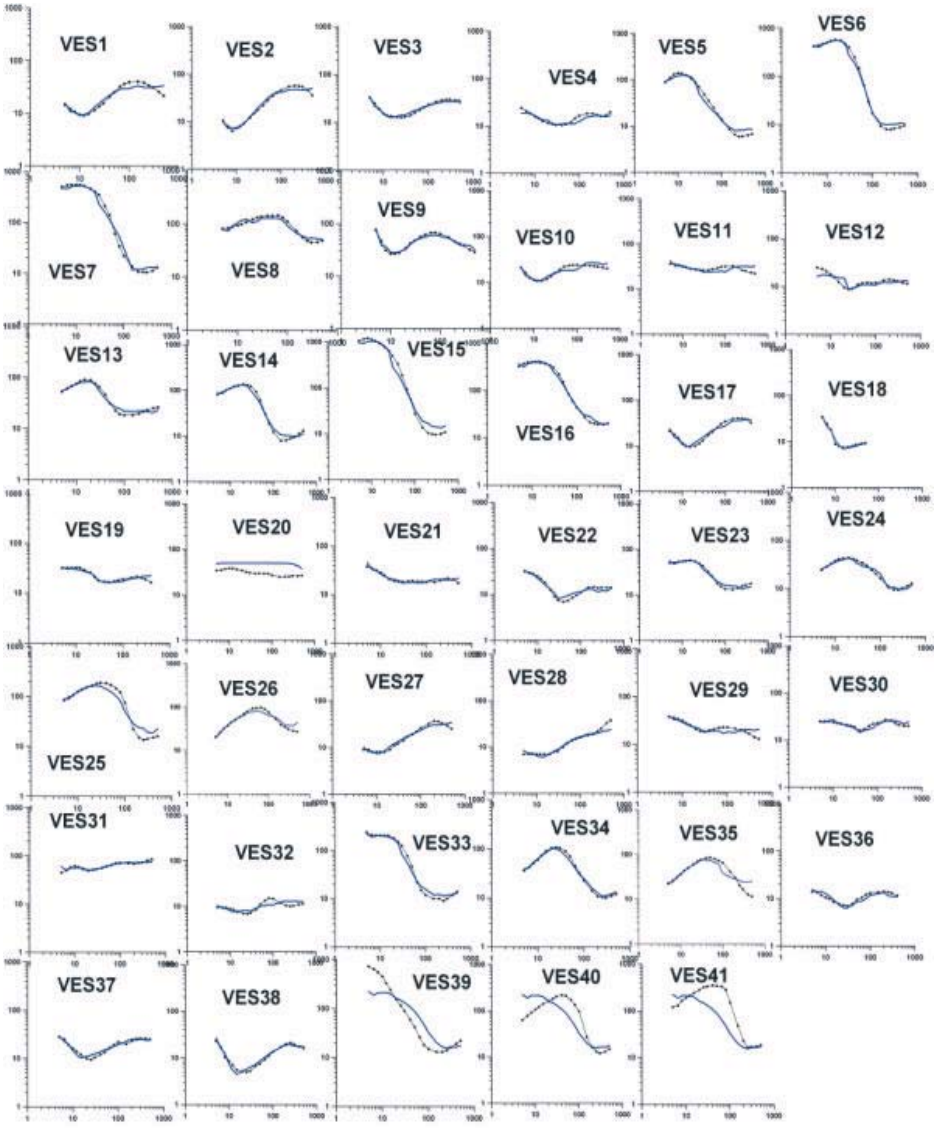

Fig. 6: Fitting of 3D VES inversion

Deep Geoelectrical Investigation Tools: The deep geoelectrical tool is represented by measuring 41 vertical electrical soundings (VES) of AB/2 ranging from 5 m to 500 m using the Schlumberger configuration (Fig.3). The data were acquired using a SYSCAL-R2 resistivity meter.

D resistivity inversion: The objective of the inversion process is to obtain a distribution of the electrical resistivity (model) whose response approaches the field data (apparent resistivity values) within the limits of data errors and that correlates well with all available data, especially the geological information [9]. The smoothness-constrained least-squares method has been widely used in 2-D and 3-D inversions of magnetotelluric, electromagnetic and geoelectrical data sets [13-16]. The scheme adopted in this study is based on [15,16]. The dc resistivity inverse problem can be expressed as

$$J \Delta p = \Delta d \quad (1)$$

where Δp is the vector containing the corrections to the model parameters p, $\Delta d = y^c - y^{ob}$ is the vector of the differences between the model responses and the measured data and J is the derivative matrix (Jacobian) containing the derivatives of the model responses. In the present study forty-one were inverted by using a new approach, the full description for this approach was

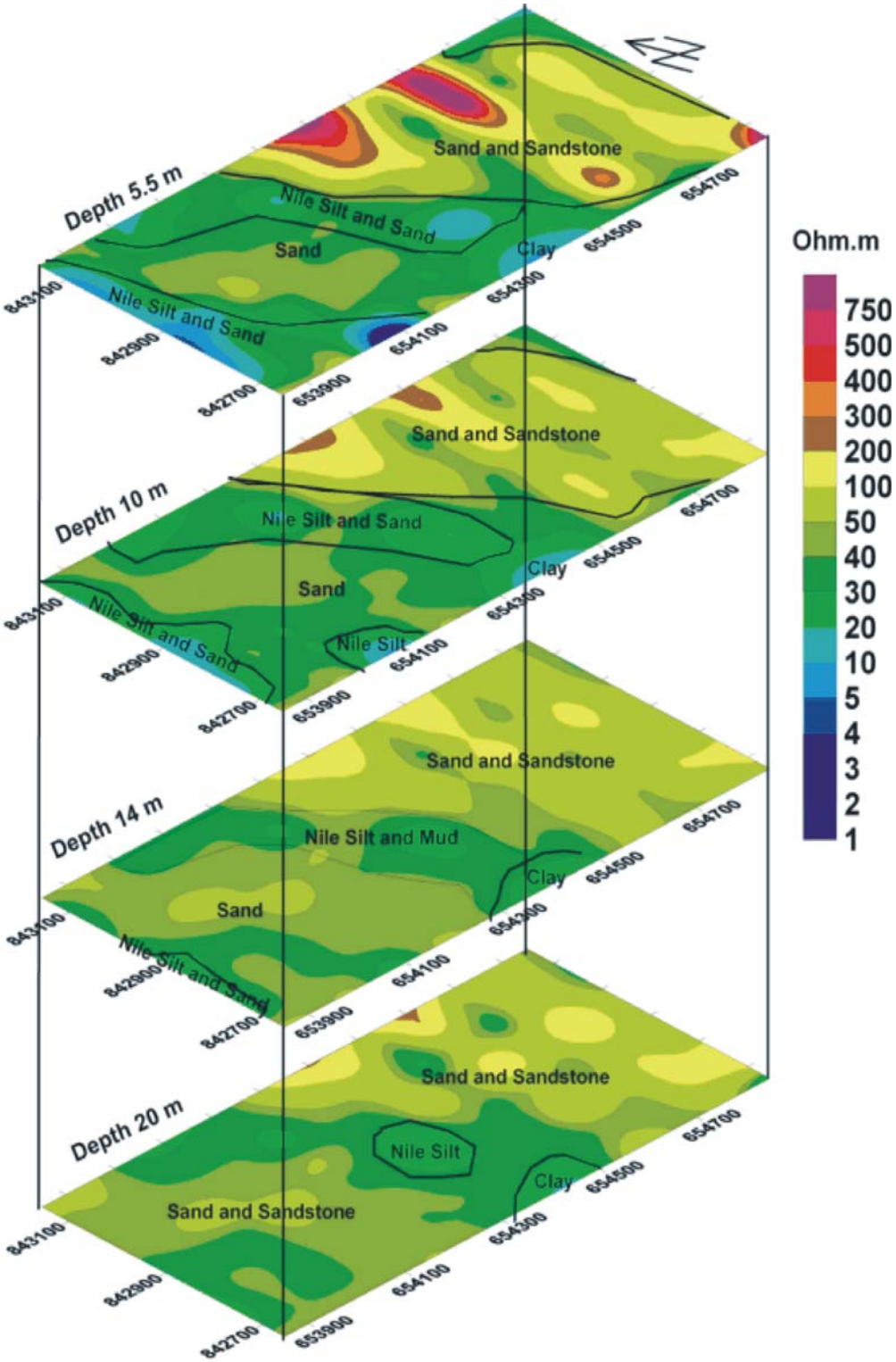

Fig. 7: 3D VES inversion slices at depth 5.5, 10, 14 and 20 m.

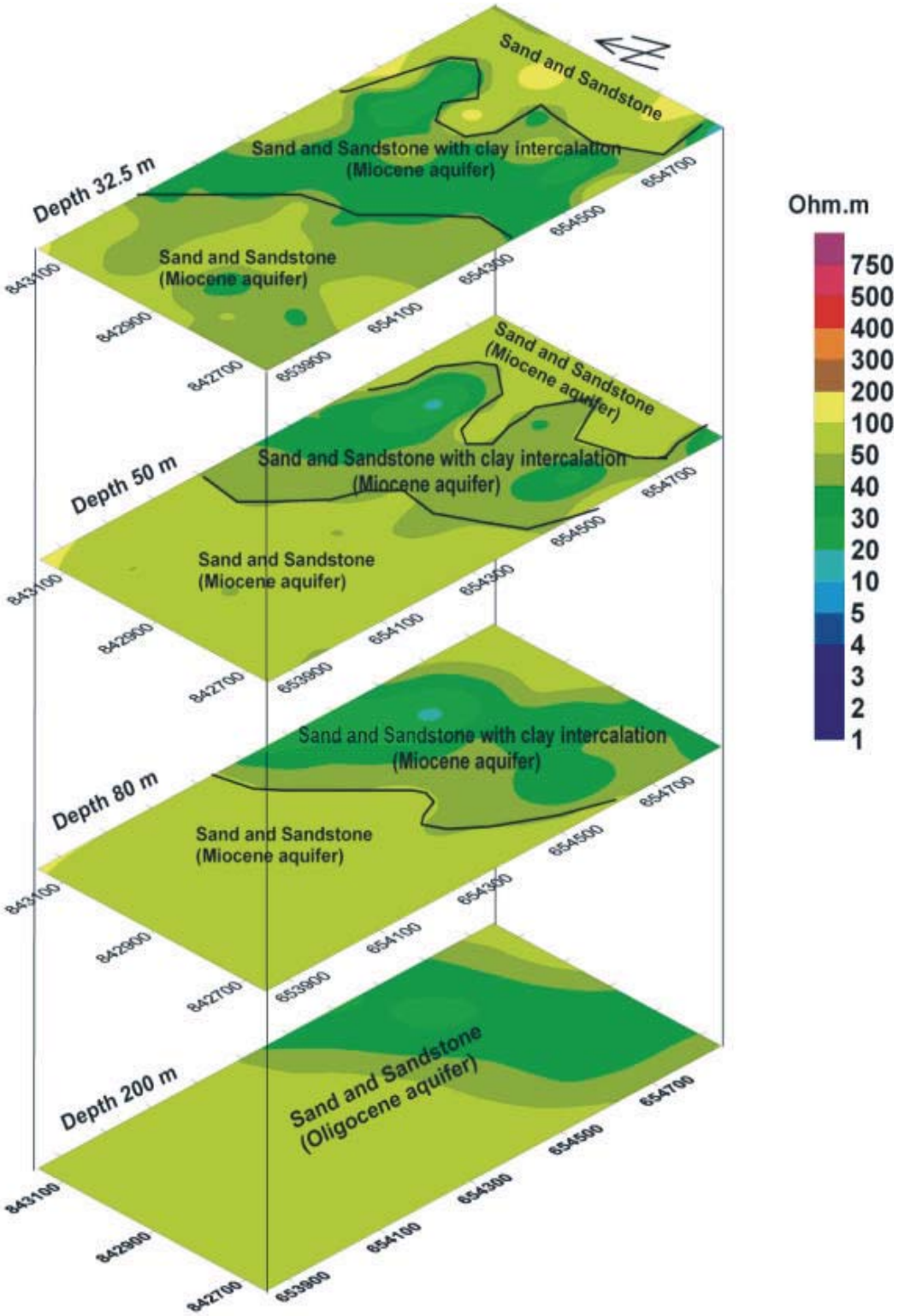

Fig. 8: 3D VES inversion slices at depth 32.5, 50, 80 and 200 m

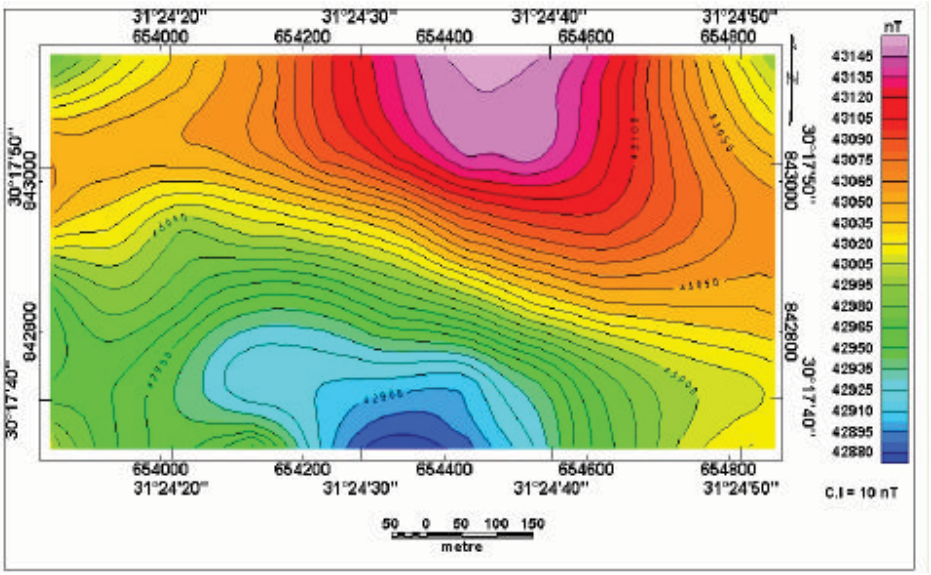

Fig. 9: Total intensity magnetic map

presented in [10]. The results of the 3D inversion firstly represented by Figure 6 which shows the comparison between measured and calculated apparent resistivity curves. The misfit between data and model responses is a good fitting for most VES stations with rms error less than 10 % except the VES stations no.20, 39, 40 and 41 exhibit bad fitting.

3D Resistivity (VES) Inversion Slices: The resistivity depth slices for the results of 3D inversion for VES data indicate that the study area show large variation in resistivities according to lithologic composition. 3D slice at depth 5.5 m exhibits very low resistivities ranging from 4-20 ohm.m according to Nile silt and Nile mud at the western and central part of the area, the low resistivities ranging from 30-50 ohm.m occupying the eastern part corresponding to sand. The eastern part of the area reveals high and very high resistivities ranging from 100-750 ohm.m for sand and sandstone. The depth slice at 10 m exhibits low resistivities corresponding to sand, Nile silt and Nile mud at the western part of the area, the eastern part reflects high resistivities according to sand and sandstone. The depth slices at 14 and 20 m show variation in resistivities ranging from 20-200 ohm.m corresponding to sand, Nile silt, Nile Mud and sandstone. The Miocene groundwater aquifer appears at depth slice 32.5 at the most study area where the Miocene aquifer consists of sand and sandstone of clay intercalation at the central part and the western part, the aquifer composed of sand and sandstone of moderately resistivities. The eastern part represents the dry Miocene sand and sandstone of high resistivities ranging from 50-100 ohm.m. The slices at depths 50 and 80 m represent the Miocene aquifer which cover all the area and composed of clayey sand and sandstone at the central part but the eastern and western part occupying by sand and sandstone. The basaltic sheet is not represented in 3D VES slices where the depths of basalt ranging between 80 and 120 m and 3D slices were represented by slices at depths 5.5, 10, 14, 20, 32.5, 50, 80 and 200 m (Figs.7 and 8).

Magnetic Data: The magnetic data in the present study were represented by measuring 221 ground magnetic stations using two proton magnetometers (Envimag made by Scintrx), one used for diurnal variation corrections at the base station and the second instrument was used for field work recording. After removing the diurnal variation from the field data, the magnetic data were contoured by Oasis Montaj [17], the final picture represents the total intensity magnetic map (Fig.9). The total intensity map indicates that the northern part occupying by high magnetic ranging from 43005-43145 nT and the southern part represents by low magnetic values ranging from 42880-43005 nT. The total magnetic fields which can be created by geological bodies are distorted by the inclination and declination of the earth's field making difficult to estimate correctly the shapes and locations of these magnetized bodies. In order to overcome this distortion in the appearance of an anomaly, a mathematical procedure is adopted on a grid of

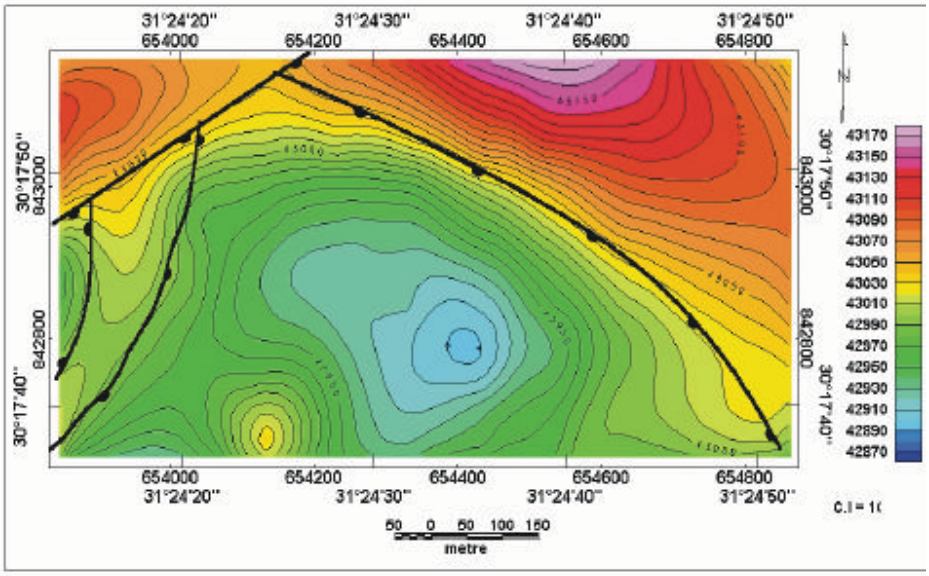

Fig. 10: Total intensity magnetic map reduced to the pole complied with the interpreted faults

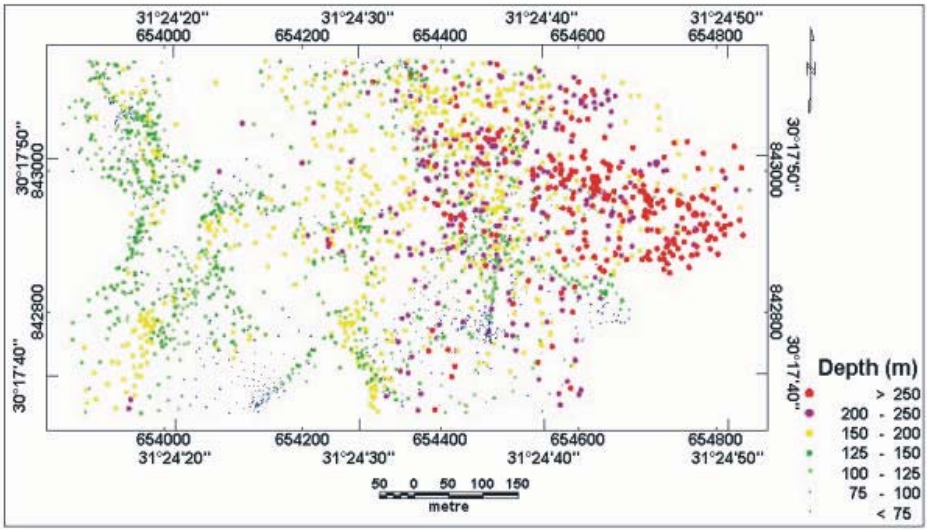

Fig. 11: Euler depth solutions

values of the contour map of the total magnetic intensity. Therefore, the interpretation of the magnetic data starts with the conversion of the total intensity map into a more interpretable map: then reduced to magnetic pole map. This mathematical procedure was first described by [18-22]. The total intensity magnetic map reduced to the pole (Fig.10) shows that the northeastern and northwestern parts occupying by high magnetic up to 43170 nT, the southern and central parts reflect low magnetic. This map was used to delineate the structural elements which dissect the study area; these fault elements have NW-SE, NE-SW and N-S trends (Fig.10).

Magnetic Depth Estimation: Magnetic data was used to determine the depth of the top of the basaltic sheet. The quantitative interpretation of the total intensity magnetic map reduced to the pole is carried out by using GRIDEPTH program which is part of the [17]. The method used in the program is based in the Euler's homogeneity equation. The Euler's homogeneity equation relates the field (magnetic) and its gradient components to the location of the source, with the degree of homogeneity N, which may be interpreted as a structural index [23]. The structural index is a measure of the rate of change of a field with distance.

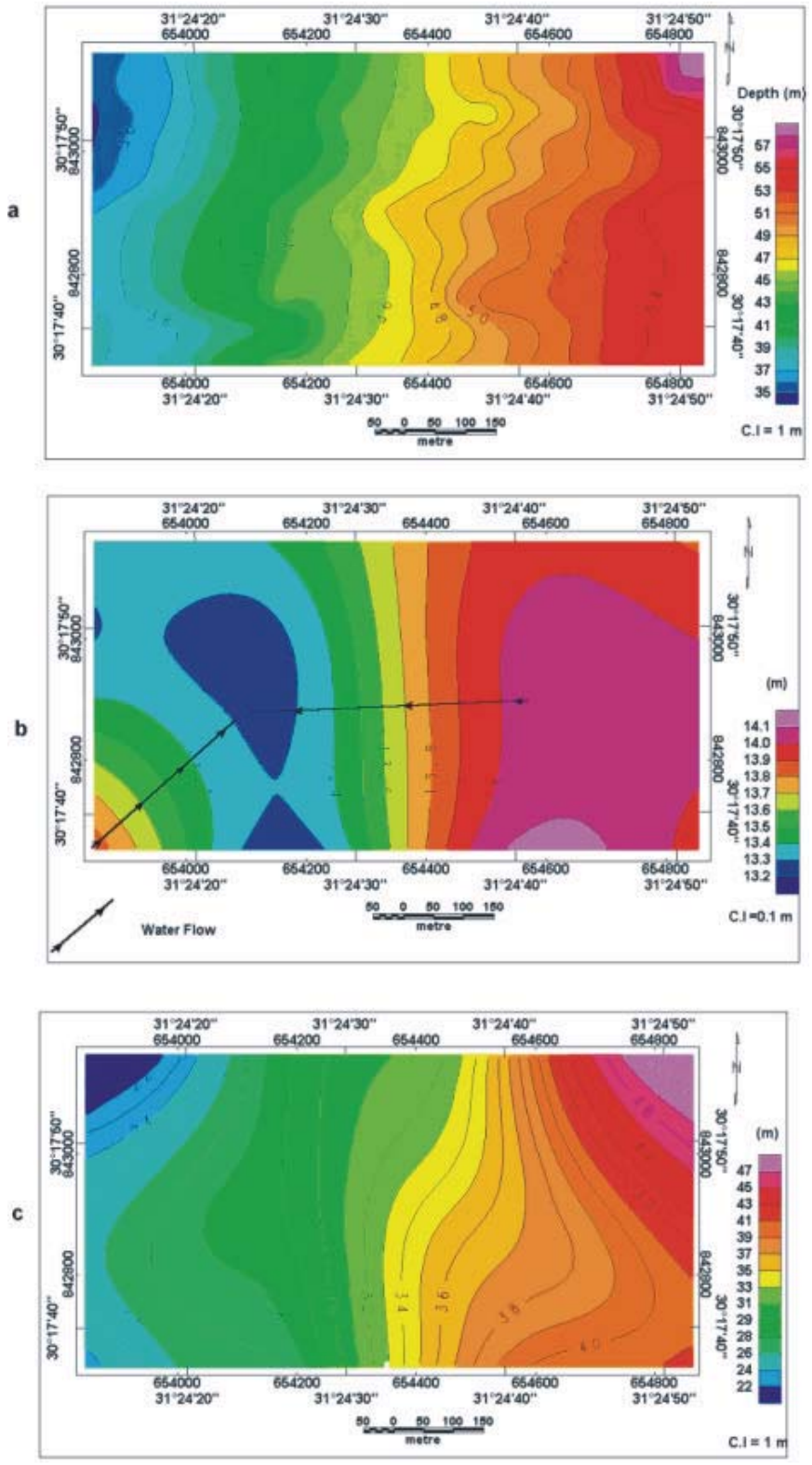

Fig. 12a-c: a) Topographic map, b) Water table map and c) Water depth map.

Table 1: Hydrochemistry data collected from drilled boreholes in the study area

	Borhole1	Borhole3	Borhole7	Borhole9	Borhole11	Borhole15
Cl^- mg/L	261	516.4	329.1	624.2	39.7	493
SO_4^{--} mg/L	184.8	326	314.1	677.3	88.6	350.3
HCO_3 mg/L	247.1	271.5	222.7	198.3	247.1	247.4
Na^+ mg/L	307.9	488	375.2	553.2	121.4	482.2
K^+ mg/L	9.1	13.8	8.9	15.7	7.8	9.9
Ca^{++} mg/L	20.7	51.7	39.6	75.8	27.6	44.8
Mg^{++} mg/L	7.3	19.8	11.4	59.3	18.7	21.8
TDS mg/L	1037.9	1687.2	1301	2213.8	550.9	1650.1
TH mg/L	330.5	348	290.3	593.5	351.2	314
PH mg/L	7.61	7.77	7.86	7.85	7.86	7.54
EC μ mho/cm	850	1250	1000	3250	700	1300
Total Hardness (mg/l)	27.551	50.194	46.596	108.461	16.705	54.056
Water table (m)	13.58	13.8	13.28	14.05	13.84	14.3
Total depth (m)	50	50	75	128	50	50
Elevation (m)	34	44.8	42	51.5	37.5	55.6

The authors were used structural index (SI) equal 1 where the source of magnetic anomaly is a basaltic sheet which represents a sill at different depths through the study area, as shown in borehole description (Fig.2). The Euler solutions were represented by Figure 11 which indicates that the western part of the area occupying by shallow depths of basalt ranging from 75 to 125 m and the central and eastern parts represent the deep depths for the basaltic sheet ranging from 125 to 250 m.

Hydrogeology of the Study Area: Hydrogeology is the branch of geology that deals with the occurrence, distribution and effect of groundwater. Some hydrogeologcal studies were carried out on the study area such as flow measurements to get an idea of water flow along the Ismailia Canal course and quantity of water which seeps into the groundwater from the canal, the measurements were carried by [24] along section of length 28 km between Abu Zabal south study area (upstream) to Belbies north study area (down-stream). The results of the measurement indicated that the velocity of water in Canal is 0.87 m/s, a section area = 51.5 m^2, amount of seepage = 45 m^3/s for the upstream and an section area = 90 m^2, a velocity = 0.45 m/s, amount of seepage = 40.5 m^3/s for the down stream. The measurements indicated also, the side flow input = 0 m^3/s and output side flow = 4.13 m^3/s. The measurements include also 10 tests for estimating the hydraulic conductivity, the results of tests indicated the hydraulic conductivity is 0.102, 0.265, 1.233, 1.427, 0.081, 0.061, 0.0815, 1.019, 0.112 and 0.122 cm/min. Water table was estimated through seven boreholes no. 1, 3, 5, 7, 9, 11 and 15 as shown in Table 1.

The topographic map (Fig.12a) of the study area was constructed using elevation measurements which were carried out by using a Leica TC805 "Total Station" instrument of high resolution and good readability under all light conditions, where the study area is characterized by gentle slop from east (57 m) to west (35 m). Water table map (Fig.12b) shows two gentle gradients, the first from east to west and the second located at the southeast part of the area where the water table varied from 13.2 to 14.1 m. The water table map indicates that the recharge source is Ismailia canal from southeast part and Miocene aquifer at the eastern part. Figure 12c reflects the depth of water ranging from 21 at the northwest part to 49 m at the northeast part.

Porosity Estimation: The porosity of the aquifer for clay free can be estimated through the equation 1 (Mark and Uri, 2004)

$$\rho_w = \rho_b \Phi^2 \quad (1)$$

Where the ρ_b is the bulk resistivity of the rock, ρ_w is the resistivity of water within the pore space, Φ is fractional porosity of the rock (approximately representing the volume of water filling the pore space), but the study area contains clay according to the boreholes results (Fig. 2), [25] summarized an equation for estimating the porosity through the bulk conductivity and groundwater conductivity for the aquifer contains clay (clayey sand and clayey sandstone), parameters in this equation are shown in equation 2:

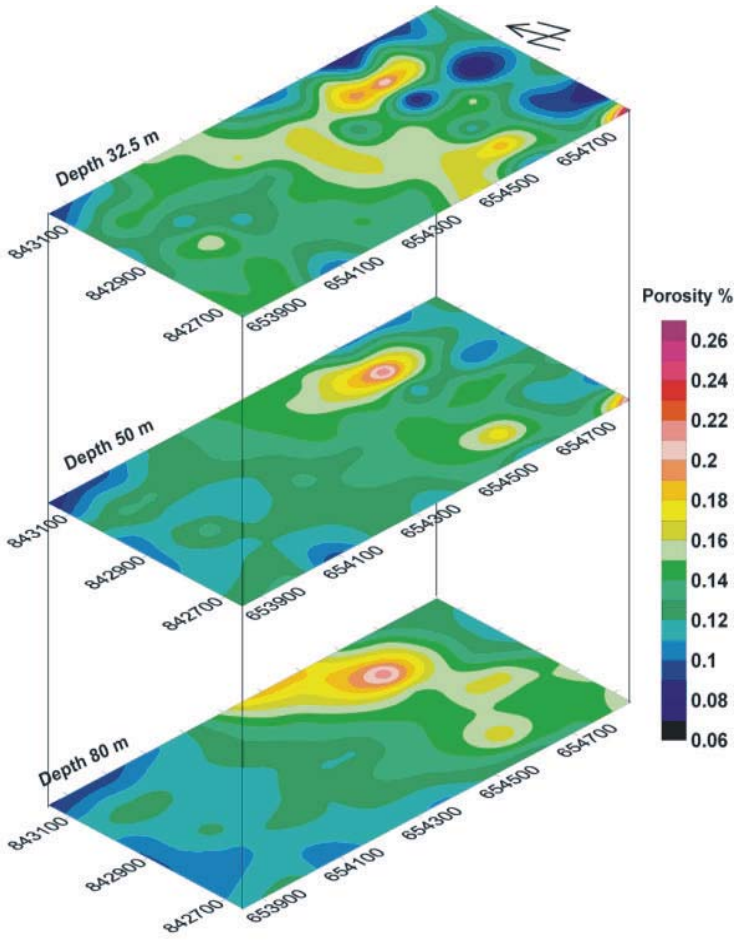

Fig. 13: Porosity percentage of the Miocene aquifer at depths 32.5, 50 and 80 m.

$$\sigma = \Phi^m \{ \sigma_w + AQ_v/(1+CQ_v/\sigma_w) \} \quad (2)$$

Where σ is the conductivity of the aquifer, σ_w is water conductivity, Φ is porosity of the aquifer, *m, A* and *C* are constants Q_v the clay charge contribution per unit pore volume. Sen *et al.,* determined these parameters through 140 core samples as the following *m*= 2, *A*= 1.93x*m* (mho/m)(1/mol), Q_v = 2.04 and CQ_v = 0.7 (mho/m). σ_w was estimated through boreholes which drilled in the study area, the average values of σ_w is 0.119 s/m, the results of porosity estimation of the Miocene aquifer were represented by Figure 13. The slice at depth 32.5 m (Fig.13a) reveals low porosity percentage at the eastern part ranging from 0.08 to 0.11 %, but the central part shows high porosity percentage ranging from 12 to 23 %. The porosity distribution at depth 50 m (Fig.13b) exhibits low porosity percentage at the eastern and western parts, the central part reveals high porosity 23 %. The porosity percentage at depth 80 m indicates that the most study area has high porosity percentage (13-23 %).

Hydrochemistry of the Area: The hydrochemistry of the water has been described through six samples of water were taken from the boreholes and listed in table (1). The total dissolved salts (TDS) were representing by salinity map (Fig.14a) which indicates that the central part is occupying by high salinity (2200 mg/l) and the southwestern part reveals low salinity about 550 mg/l.

Water Type: The type of water is detected through the representation of boreholes data through Piper trilinear diagram and ratios of main ions in water chemistry through Schoeller diagram, where theses diagrams indicate that the water type is Na-Cl-SO4 for boreholes 3, 7 and 9; Na-HCO3-SO4 for boreholes 11 and 15; Na-Cl-HCO3-SO4 for borehole 1 (Fig14b). The ratios of

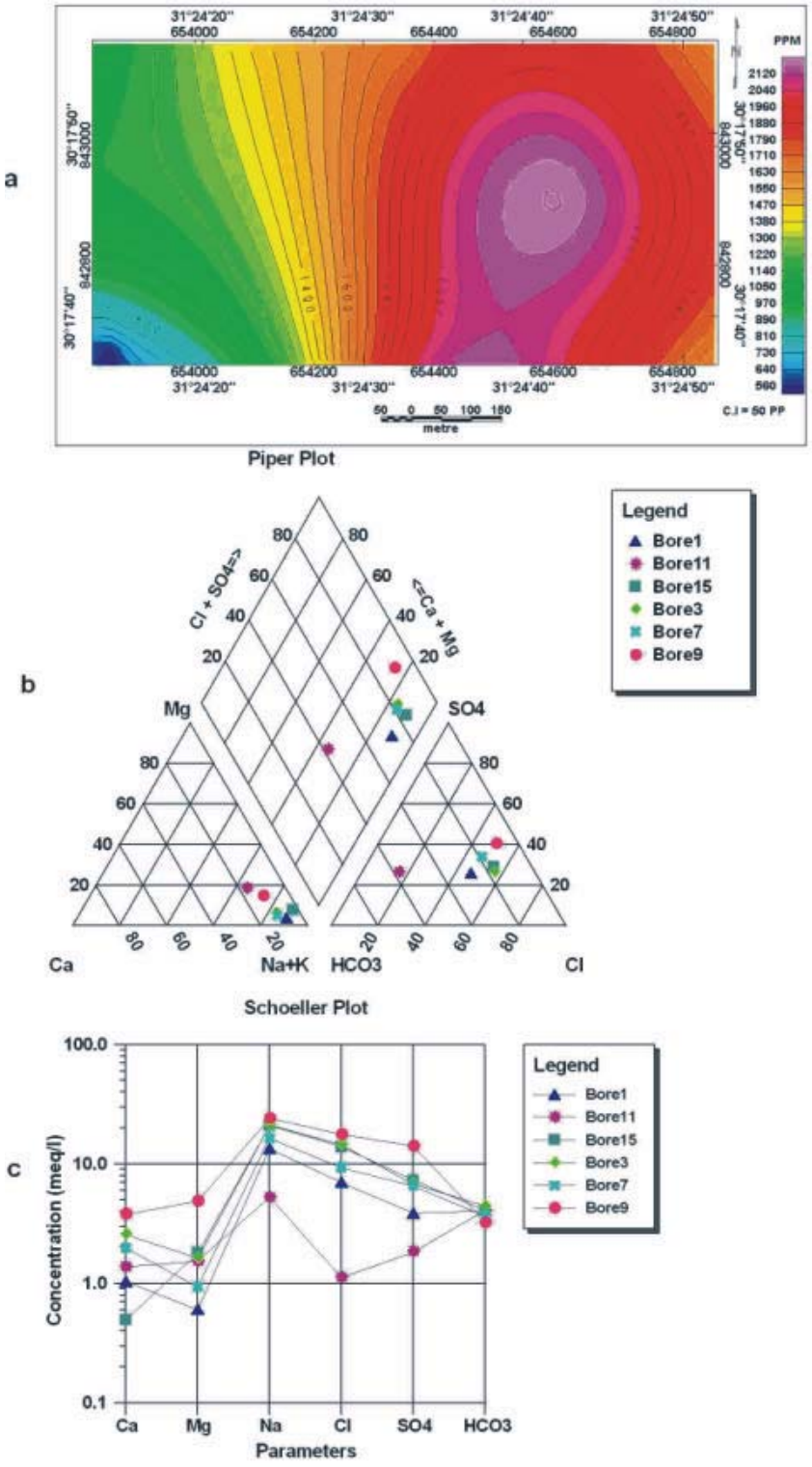

Fig. 14a: Salinity map, b: Pieper Diagram and c: Schoeller diagram.

ions are higher for the borehole 9 and the lower ratios of ions are for Borehole 11 (Fig.14c). The total hardness have been estimated through the following equation [26].

$$\text{Hardness } (H_{tot}) = 0.14*Ca^{+2} + 0.23* Mg^{+2} \quad (3)$$

The results of hardness estimation has been tabulated in table (1), the result indicate that the total hardness of water is a slightly hard (17.1-60), but the borehole 9 exhibits 108.5 mg/l (moderately hard).

DISCUSSION

The 3D representation for dipole dipole data at depth 5.7 m (Fig.5) is compatible with 3D VES inversion at depth slice 5.5 where the eastern part exhibits high resistivities corresponding to sand and sandstone while the western part reveals low resistivities corresponding to Nile silt and mud with sand. All depth slices of the resistivity are compatible with results of borehole data (Fig.2). The depth of the upper surface of basalt from boreholes data refers for increasing the depth from west to east and the interpretation of magnetic data indicates that the Euler solutions for depth were increased from west to east where the central and eastern parts reveal high depth ranging from 125-250 m. The slices of 3D VES inversion at depth 32.5, 50 and 80 m reveals low resistivities corresponding to Miocene aquifer. The variation of the depth of the basaltic is according to the fault elements which dissected the area and shown in figure 9. The salinity map (Fig.14a) is compatible with the depth slices of the 3D VES inversion at depth 32.5, 50 and 80 which represent the Miocene aquifer where the central part reveals high salinity and low resistivities. The low salinity at the southwestern part refers to the recharge of the aquifer is coming from Ismailia canal (fresh water).

CONCLUSION

Through the interpretation of the geophysical and hydrogeologicat data we can concluded that the shallow part of the stratigraphic section of the study area consists of Nile silt, Nile mud and clay while the eastern part exhibits high resistivities corresponding to sand and sandstone for this reason the eastern part of the study area is suitable for constructions The depth of the Miocene aquifer is ranging from 32.5 to 80 m, the quality of the water is good and suitable for drinking and agricultural purposes where the salinity ranging from 550-2200 gm/l and the total hardness is ranging between 16.7-108.5 gm/l. The depth of the basaltic sheet ranging from 75 to 250 m. The area dissected by fault elements of NW-SE, NE-SW and N-S trend.

REFERENCES

1. Keller, G.V. and F.C. Frischknecht, 1996. Electrical methods in geophysical prospecting, Pergamon Press.
2. Telford, W.M., L.P. Geldart and R.E. Sheriff, 1990. Applied Geophysics (2nd Edition), Cambridge University Press.
3. Ward, S., 1990. Resistivity and induced polarization methods, in Ward, S., Geotechnical and environmental geophysics, Vol.1: SEG Investigation in geophysics, 6: 147-189.
4. Laurence Bentley and Mehran Gharibi, 2004. Case study, Two-and three-dimensional electrical resistivity imaging at a heterogeneous remediation site, Geophysics, 69(3): 674-680.
5. Loke, M.H. and R.D. Barker, 1996a, Practical techniques for 3D resistivity surveys and data inversiton: Geophysical Prospecting, 44: 499-523.
6. Loke, M.H. and R.D. Barker, 1996b. Rapid least-squares inversion of apparent resistivity pseudo-sections using quasi-Newton method: Geophysical Prospecting, 44: 131-152.
7. Rijo, L., 1984. Inversion of three-dimensional resistivity and induced-polarization data: 54th Ann. Internat. Mtg., Soc. Expl. Geophys., Expanded Abstracts, pp: 113-117.
8. Li, Y. and D.W. Oldenburg, 1992. Approximate inverse mappings in DC resistivity problems: Geo. Hys. J. Int., 109: 343-362.
9. Sultan, S.A. and F.A. Monteiro Santos, 2008. 1-D and 3-D Resistivity Inversions for Geotechnical Investigation, J. Geophys. Eng., 5: 1-11.
10. Mark Goldman and Uri Kafri, 2004. Hydrogeophysical Applications in Coastal Aquifers, Applied Hydrogeophysics, NATO Science Series, published by IOS Press, Amsterdam.
11. Monteiro Santos, F.A. and S.A. Sultan, 2008. On the 3-D inversion of Vertical Electrical Soundings: application to the South Ismailia-Cairo Desert Road area, Cairo, Egypt, J. Appl. Geophysics, 65: 97-110.
12. Edwards, L.S., 1977. A modified pseudosection for resistivity and induced polarization. Geophysics, 42: 1020-1036.

13. DeGroot-Hedlin, C. and S.C. Constable, 1990. Occam's inversion to generate smooth, two-dimensional models from magnetotelluric data. Geophysics, 55: 1613-1624.
14. Sasaki, Y., 1989. Two-dimensional joint inversion of magnetotelluric and dipole-dipole resistivity data. Geophysics, 54: 254-262.
15. Sasaki, Y., 1994. 3-D resistivity inversion using the finite element method. Geophysics, 59(12): 1839-1848.
16. Sasaki, Y., 2001. Full 3-D inversion of electromagnetic data on PC. J. Appl. Geophysics, 46: 45-54.
17. Geosoftw Program (Oasis Montaj), 1998. Geosoft mapping and application system, Inc, Suit 500, Richmond St. West Toronto, ON Canada N5SIV6.
18. Baranov, V., 1957. A new method for interpretation of aeromagnetic maps: pseudo gravimetric anomalies. Geophysics, 22: 359-383.
19. Baranov, V., 1975. Potential fields and their transformation in applied geophysics. Geoexploration Monographs, series 1-6, Gebrüder, Borntraeger, Berlin-Stuttgart.
20. Baranov, V. and H. Naudy, 1964. Numerical calculation of the formula of reduction to the magnetic pole, Geophysics, 29: 67-79.
21. Bhattacharyya, B.K., 1967. Some general properties of potential field in space and frequency domains; A review Geoexploration, 5: 127-143.
22. Bhattacharyya, B.K., 1965. Two dimensional harmonic analysis as a tool for magnetic interpretation ; Geophysics, 30(5): 829-857.
23. Thompson, D.T.T., 1982. Euler, a new technique for making computer assisted depth estimates from magnetic data, Geophs., 47: 31-37.
24. Geological Survey of Egypt (EGSMA), 1998. Geology of Inshas Area, Geol.Surv. of Egypy, internal report
25. Sen, P.N., P.A. Goode and A. Sibbit, 1988. Electrical conduction in clay bearing sandstones at low and high salinities. J. Appl. Physics, 63(10): 4832-4840
26. Reinhard, K., 2004. Groundwater Geophysics, A Tool for Hydrogeology, text book, ISBN 10 3-540-29383-3 Springer Berlin Heidelberg New York.